Linear polarization conversion of transmitted terahertz wave with double-layer meta-grating surfaces

Han Sun (孙 翰)[1], Yaxin Zhang (张雅鑫)[1,*], Kailong Wang (王开龙)[1], Yuncheng Zhao (赵运成)[1], Wei Kou (寇 伟)[1], Shixiong Liang (梁士雄)[2,], Jiaguang Han (韩家广)[3], and Ziqiang Yang (杨梓强)[1]**

[1]*Terahertz Science Cooperative Innovation Center, University of Electronic Science and Technology of China, Chengdu 610054, China*

[2]*National Key Laboratory of Application Specific Integrated Circuit, Hebei Semiconductor Research Institute, Shijiazhuang 050051, China*

[3]*Center for Terahertz Waves, College of Precision Instrument and Optoelectronics Engineering, Tianjin University, Key Laboratory of Optoelectronic Information Technology (Ministry of Education), Tianjin 300072, China*

**Corresponding author: zhangyaxin@uestc.edu.cn; **corresponding author: wialliam@163.com*

Received May 2, 2018; accepted June 13, 2018; posted online July 30, 2018

In this Letter, we demonstrate a linear polarization conversion of transmitted terahertz wave with double-layer meta-grating surfaces, which integrated the frequency selectivity of a split ring resonator metasurface and the polarization selectivity of a metallic grating surface. Since the double-layer can reduce the loss, and the Fabry–Perot like resonant effect between the two layers can improve the conversion efficiency, this converter can rotate the incident y-polarized terahertz wave into an x-polarized transmitted wave with relatively low loss and high efficiency. Experimental results show that an average conversion efficiency exceeding 75% from 0.25 to 0.65 THz with the highest efficiency of 90% at 0.43 THz with only −2 dB loss has been achieved.

OCIS codes: 160.3918, 050.2230, 350.2770.
doi: 10.3788/COL201816.081601.

Terahertz (THz) science and technology has rapidly been becoming the focus in the fields of information and communication technology, sensing, and imaging[1–7]. Most of the applications need not only highly efficient THz sources but also sophisticated devices, such as lenses, switches, and polarization converters[3–10]. As polarization is critical in many THz applications, such as THz spectroscopy, THz imaging systems, and THz radar systems, manipulation of the polarization of a THz wave attracted more and more concerns.

Since the choice of THz responsible materials is limited, the development of THz polarizing optical elements is far inferior to its counterpart in the optical/infrared regime. By applying the concept of metamaterials, the polarization of the THz wave can be flexibly controlled; so, over the past decade, artificially engineered subwavelength metamaterials have opened up tremendous opportunities to develop versatile THz polarization converter devices offering great control at the unit cell level. Most of these metasurface polarization converters operate in the reflection mode[11–13]. The devices in the reflection mode could not fulfill the general demands of different kinds of THz application systems, e.g., Gao *et al.* presented an ultrawideband and high-performance polarization converter that uses a double V-shaped metasurface[14]. Therefore, recently, the direction of polarization conversion in the transmission mode has been intensively studied, as shown in Refs. [15–18]. Nevertheless, it can be found that most of the conversion in the transmission mode is by utilizing a multi-layered structure with more than three layers. Xu *et al.* showed that in the frequency range of 0.2 to 0.4 THz, the three-layer polarization converter had a fat transmission curve and exhibits a transmission efficiency that is higher than 80%[19]. Several progresses focus in the one- or double-layer structure, such as the one layer with a complementary metasurface that has been proposed to realize a simpler structure or is composed of the subwavelength Si grating and metallic wire grating layers[20–22]. Cong *et al.* realized the dispersion-free operation of a phase engineered metadevice by integrating two grating-based metasurfaces that are designed by using phase dispersion compensation[23]. In addition, Xu *et al.* designed the polarization mode converter based on the compound metasurface combined with a dielectric grating and a metallic metamaterial. Different polarization code conversions from a TM to a TE resonance mode occur at 1.3 THz for forward transmission and 0.63 THz for backward transmission[24]. The practical application is limited for the narrow bandwidth. As we know, due to the dielectric loss, scattering, and diffraction loss, more layers could lead to higher loss and a more complicated fabrication process[25–27]. In addition, the loading of metal structures on heterogeneous materials can also achieve polarization conversion by changing the electromagnetic properties of materials. Fan *et al.* found that longitudinally magnetized InSb can be applied to the circular polarizer and nonreciprocal one-way transmission for the circular polarization THz waves[28]. However, there are difficulties in processing and designing heterosexual materials. Therefore, in order to achieve higher efficiency, lower loss, and a simpler

fabrication process, in this Letter, linear polarization conversion of the THz wave with double-layer meta-grating surfaces in the transmission mode has been proposed. By combining the advantages of agile frequency selectivity of a split-ring resonator (SRR) metasurface and the polarization selectivity of a traditional metallic grating surface, more than 75% average conversion efficiency and only −2 dB loss have been achieved from the 0.25 to 0.65 THz frequency band with the highest efficiency of 90% at 0.43 THz. Moreover, it has been found that by adjusting the unit cell of the metamaterial, the frequency band can be precisely controlled.

The schematic of the linear polarization conversion of the transmitted THz wave with the double-layer meta-grating surfaces structure is illustrated in Fig. 1(a). The y-polarized THz wave perpendicularly transmits through the double-layer structure; meanwhile, the x-polarized THz wave can be detected. The unit cell structure is shown in Fig. 1(b), the upper layer is just a circular split-ring oriented with a 45° angle metasurface, and the lower layer is just a traditional wire-grid surface. The designed size parameters are $r = 100$ μm, $w = 10$ μm, $d = 20$ μm, and the period of each unit is $P_x = 210$ μm, $P_y = 210$ μm. The lower layer is composed of metallic gratings, which are parallel to the y axis, and the structure parameters are $a = 20$ μm and $b = 10$ μm. Considering the low insertion loss characteristic, the quartz with a thickness of 100 μm has been utilized for substrate. Following the photolithography, electron-beam metal deposition, high-accuracy alignment, and lift-off fabrication process, the upper and lower metasurfaces with 200 nm gold metal can be achieved, as shown in Figs. 1(c) and 1(d). As shown in Fig. 1(c), the gray part is quartz, and the white part is a metal ring. In Fig. 1(d), the gray part is quartz, and bright yellow part is a metal grating.

Next, the THz time-domain spectroscopy (TDS) with an independent tunable transmitter and receiver was used to characterize the THz wave polarization conversion performance of this two-layer structure in the transmission mode. In this system, the transmitter and receiver can be rotated separately to detect the polarization conversion. The system is shown in Fig. 2(a). In the case of the y-polarized incident wave, in order to get the cross-polarization transmission rate, the receiver should be rotated to x polarization. The measured results of the time-domain signal on the reference and cross- and co-polarization of the sample are shown in Fig. 2(b). The cross-polarized transmission coefficient is defined as $T_{xy} = |E_x^{\text{out}}|/|E_y^{\text{in}}|$, relating to the incident (E_y^{in}) and transmitted (E_x^{out}) waves. The first and second subscripts of the coefficients (T_{xy} or T_{yy}) denote the transmitted and incident polarization, respectively. The letter E represents the magnitude of the electric field, and the superscript and subscript represent the direction of the wave and the polarization. The co-polarized transmission is defined as $T_{yy} = |E_y^{\text{out}}|/|E_y^{\text{in}}|$.

By applying the fast Fourier transformation (FFT), the spectrum can be obtained, as in Fig. 2(c). In these figures, the T_{xy} and T_{yy} exhibited the y-polarization generation with the x- and y-polarization receiver, respectively. Based on the data of spectrum, the transmittance of different linear polarizations could be retrieved, as in Fig. 2(d), where the dash dot lines and solid lines display the simulation results and experimental results, respectively. For this double-layer converter, it can be found in Fig. 2(d) that the device is able to rotate the linear polarization by 90° with an average conversion coefficiency T_{xy} exceeding 75% from 0.25 to 0.65 THz with the highest efficiency of 90% at 0.43 THz. The co-polarized transmittance T_{yy} is mostly less than 20% and approaches 10% at some frequencies, demonstrating the capability of

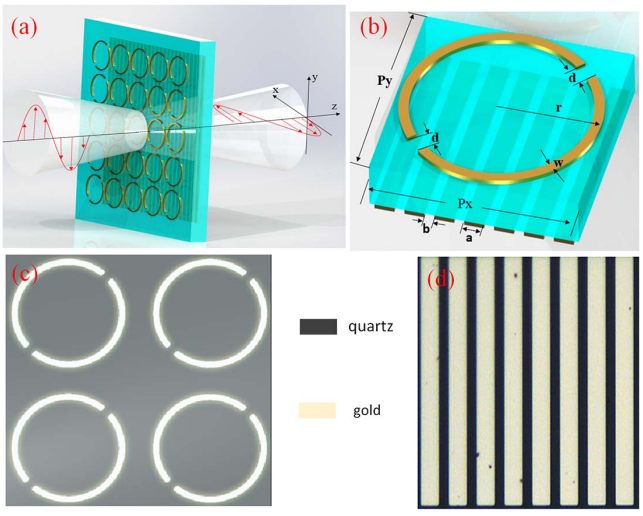

Fig. 1. (a) Schematic of the sample used in the experiment. (b) The size parameters of the unit cell. (c) The photos of the manufactured metasurface. (d) The photos of the manufactured grating layer.

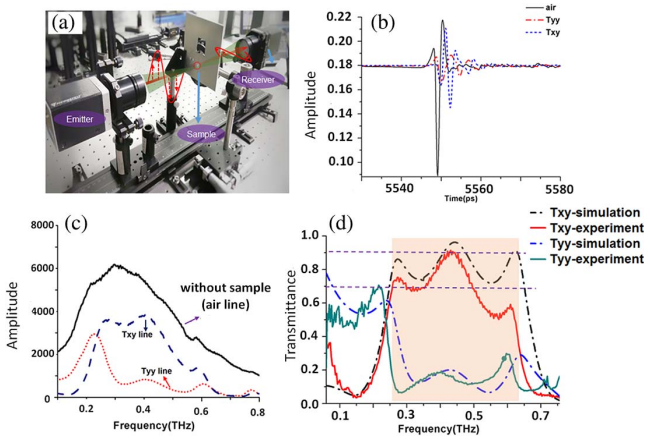

Fig. 2. (a) TDS experimental test system. (b) Time-domain waveform. (c) The FFT of the time-domain signal of the air sample, the cross-polarization coefficient (T_{xy}), and co-polarization coefficient (T_{yy}), respectively. (d) Transmittance spectra of simulated results (solid strips) and measured results (dotted strips).

rotating the input linear polarization by 90° with high output purity. The results also depict that the polarization conversion of the transmitted THz wave with about 60% bandwidth is experimentally realized. Moreover, there is a good agreement between the experimental and simulated results; meanwhile, a small difference between the simulated and measured results is due to the mismachining tolerance in the lithography process.

In order to gain insight into the nature of the polarization conversion mechanism, the three-dimensional (3D) computer simulation technology (CST) microwave studio software has been employed to simulate and analyze the mechanism. In the simulation, the unit cell boundary condition in the x–y plane has been applied to simulate the periodic array state; meanwhile, the open condition along the z direction has been set to match the practical incident and transmitted THz wave paths.

Investigations of the electromagnetic properties of the upper SRRs metasurface and lower polarized grating array surface have been carried out, respectively.

First, we analyze the upper SRRs independently. As shown in Fig. 3(a), when the y-polarized THz wave was incident normal to the surface of this converter, the incident electric field vector E_{in} through the upper SRRs can be decomposed into two orthogonal components E_1 and E_2, oriented at 45° with respect to the x and y axes. Therefore, E_2 excites the dipolar resonance mode A with the surface current flows along the semi-ring; meanwhile, E_1 induces the quadrupole resonance mode B with split distribution along the metal wire, as shown in Fig. 3(b). If we observe the transmission rate of E_2 and E_2 polarization independently, the transmission rates are shown in the upper figure of Fig. 3(c). In this figure, it indicates that the resonant frequency of mode A is around 0.31 THz, and mode B is corresponding to 0.65 THz. More importantly, from the analysis of the parallel-polarization and cross-polarization transmission, shown in the lower figure of Fig. 3(c), it can be found that the starting point and ending point of the top band correspond to the resonant peaks of modes A and B. E_1 and E_2 should be decomposed to the directions x and y, as $E_{xy} = E_2\cos\theta - E_1\sin\theta$ and $E_{yy} = E_2\sin\theta + E_1\cos\theta$. Obviously, the conversion efficiency of the x and y directions is determined by the resonant bandwidth of E_1 and E_2.

The lower layer is a subwavelength-polarized grating array surface paralleled to the y axis. For such a grating, when the linear polarization of the incident electric field is perpendicular to the grating strips, most of the incident wave can pass through the gratings because the movement of the electrons perpendicular to the strips is cut off. Furthermore, if the polarization of the incident wave is parallel to the grating strips, the movement of electrons will be induced along the gratings, as a result, the gratings act as a full metal plate, so most of the incident wave is reflected.

Based on the electromagnetic characteristics of the upper SRR layer and lower grating surface, it can be found that, as shown in Fig. 4(a), the incident electric field E_{in} is linearly polarized in the y direction and transmitted through the upper SRRs, as mentioned above, such a transmitted wave will have both E_x and E_y components. The component E_x will pass through the metal strips, meanwhile, E_y will reflect at this surface. Therefore, the reflected component E_y goes back to interact with the SRRs' surface so that the wave reflected by the SRRs' surface contains x and y components and will be selected by the metal gratings again. Afterwards, with the waves travelling back and forth between the first and second layers repetitively, there is a formation of a Fabry–Perot like resonance between the two layers, shown in Fig. 4(a), resulting in a polarization coupling and constructive inference, thus improving the conversion coefficiency. This process also has been mentioned in Refs. [29,30]. Shown in Fig. 4(b), this bi-layered structure indeed realizes the

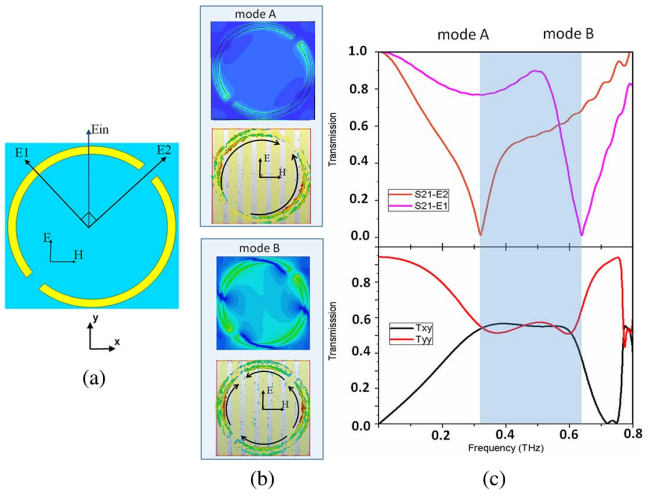

Fig. 3. (a) Decomposition of the incident electric field vector E_{in}. (b) The surface current distributions and field contours of modes A and B. (c) The transmission coefficients (S_{21}) of electric fields E_1 and E_2 and the transmission of T_{yy} and T_{xy} for just one metasurface layer.

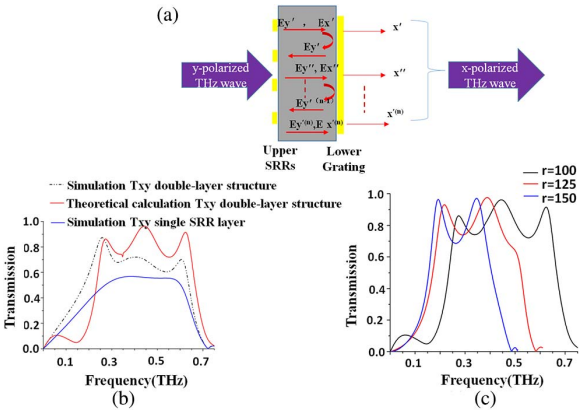

Fig. 4. (a) Scheme of the Fabry–Perot like resonance in the structure. (b) Cross-polarization conversion coefficients of the double-layer structure. (c) Cross-polarized transmission coefficients with different r.

better cross-polarization conversion than the single SRR's layer from 0.25 to 0.65 THz. Based on the theory of Ref. [21], r_{xy} and r_{yy} denote the reflection coefficients in the x and y directions when the y-polarized wave is irradiated:

$$T_{xy} \cong t_{xy}^{\mathrm{meta}} t_{xx}^{\mathrm{grat}} + \frac{t_{yy}^{\mathrm{whole}} r_{yy}^{\mathrm{grat}} r_{xy}^{\mathrm{meta}} t_{yy}^{\mathrm{grat}}}{1 - r_{yy}^{\mathrm{meta}} r_{yy}^{\mathrm{grat}}}, \tag{1}$$

where the superscripts meta and grat mean the upper metasurface and lower grating surface, respectively, and the superscript whole means the whole structure. The subscripts x and y mean x polarization and y polarization. The theoretical study results [the dot line in the Fig. 4(b)] also verified the repeating transmission reflection process.

Moreover, according to the analysis above, the polarized conversion band can be adjusted by the resonant frequency of modes A and B of the first SRR's layer, as shown in Fig. 4(c). With the decrease of the diameter of the ring, the band becomes narrow. Therefore, for this bi-layered structure, due to the resonance characteristics of the SRR's layer and polarization selection of the grating surface, efficient polarization conversion with controllable bandwidth has been achieved.

In summary, we have presented a polarization converter with a bi-layered structure, which can rotate the incident linear polarization THz wave to a 90° angle in the transmission mode. The results show that by applying the frequency selectivity of an SRR metasurface and the polarization selectivity of a metallic grating surface, an average conversion coefficiency T_{xy} exceeding 75% from 0.25 to 0.65 THz with the highest efficiency of 90% at 0.43 THz has been achieved. Moreover, it has been found that the conversion bandwidth can be controlled by adjusting the resonant frequencies of the induced mode in the first SRR's layer.

This work was supported by the National Natural Science Foundation of China (Nos. 61531010, 61270011, 91438118, and 61501094) and the National Key Basic Research Program of China (No. 2014CB339806).

References

1. V. Savinov, V. A. Fedotov, S. M. Anlage, P. A. J. De Groot, and N. I. Zheludev, Phys. Rev. Lett. **109**, 243904 (2012).
2. N. I. Zheludev and Y. S. Kivshar, Nat. Mater. **11**, 917 (2012).
3. H. Zhang, P. Guo, P. Chen, S. Chang, and J. Yuan, J. Opt. Soc. Am. B **26**, 101 (2009).
4. Y. Zhao and A. Alù, Phys. Rev. B **84**, 205428 (2011).
5. B. Scherger, C. Jördens, and M. Koch, Opt. Express **19**, 4528 (2011).
6. Q. Xu, X. Zhang, Y. Xu, C. Ouyang, Y. Li, J. Han, and W. Zhang, Chin. Opt. Lett. **16**, 050002 (2018).
7. G. Litmanovitch, D. Rrotshild, and A. Abramovich, Chin. Opt. Lett. **15**, 011101 (2017).
8. J. Liu, P. Li, Y. Chen, X. Song, F. Qi, B. Zheng, J. He, Q. Wen, and W. Zhang, Chin. Opt. Lett. **14**, 052301 (2016).
9. H.-T. Chen, W. J. Padilla, M. J. Cich, A. K. Azad, R. D. Averitt, and A. J. Taylor, Nat. Photon. **3**, 148 (2009).
10. R. Ulbricht, E. Hendry, J. Shan, T. F. Heinz, and M. Bonn, Rev. Mod. Phys. **83**, 543 (2011).
11. Y. Z. Cheng, W. Withayachumnankul, A. Upadhyay, D. Headland, Y. Nie, R. Z. Gong, M. Bhaskaran, S. Sriram, and D. Abbott, Appl. Phys. Lett. **105**, 181111 (2014).
12. X. Wen and J. Zheng, Opt. Express **22**, 28292 (2014).
13. J. Ding, B. Arigong, H. Ren, M. Zhou, J. Shao, Y. Lin, and H. Zhang, Opt. Express **22**, 29143 (2014).
14. X. Gao, X. Han, W.-P. Cao, H. O. Li, H. F. Ma, and T. J. Cui, IEEE Trans. Antennas Propag. **63**, 3522 (2015).
15. N. K. Grady, J. E. Heyes, D. R. Chowdhury, Y. Zeng, M. T. Reiten, A. K. Azad, A. J. Taylor, D. A. R. Dalvit, and H.-T. Chen, Science **340**, 1304 (2013).
16. L. Cong, W. Cao, X. Zhang, Z. Tian, J. Gu, R. Singh, J. Han, and W. Zhang, Appl. Phys. Lett. **103**, 171107 (2013).
17. R. H. Fan, Y. Zhou, X. P. Ren, R. W. Peng, S. C. Jiang, D. H. Xu, X. Xiong, X. R. Huang, and M. Wang, Adv. Mater. **27**, 1201 (2015).
18. D. J. Liu, Z. Y. Xiao, X. L. Ma, and Z. H. Wang, Opt. Commun. **354**, 272 (2015).
19. S.-T. Xu, F.-T. Hu, M. Chen, F. Fan, and S.-J. Chang, Annalen Der Physik **529**, 1700151 (2017).
20. W. Liu, S. Chen, Z. Li, H. Cheng, P. Yu, J. Li, and J. Tian, Opt. Lett. **40**, 3185 (2015).
21. Y. J. Chiang and T. J. Yen, Appl. Phys. Lett. **102**, 11129 (2013).
22. X. Liu, X. Chen, E. P. J. Parrott, and E. Pickwell-MacPherson, Photon. Res. **5**, 299 (2017).
23. X. Gao, L. Singh, W. Yang, J. Zheng, H. Li, and W. Zhang, Sci. Rep. **7**, 6817 (2017).
24. L. Cong, N. Xu, J. Han, W. Zhang, and R. Singh, Adv. Mater. **27**, 6630 (2015).
25. S.-T. Xu, F. Fan, M. Chen, Y.-Y. Ji, and S.-J. Chang, Appl. Phys. Lett. **111**, 031107 (2017).
26. J. Hao, Y. Yuan, L. Ran, T. Jiang, J. A. Kong, C. T. Chan, and L. Zhou, Phys. Rev. Lett. **99**, 63908 (2007).
27. I. Yamada, K. Takano, M. Hangyo, M. Saito, and W. Watanabe, Opt. Lett. **34**, 274 (2009).
28. F. Fan, S.-T. Xu, X.-H. Wang, and S.-J. Chang, Opt. Express **24**, 26431 (2016).
29. Y.-J. Chiang and T.-J. Yen, Appl. Phys. Lett. **102**, 011129 (2013).
30. H.-T. Chen, Opt. Express **20**, 7165 (2012).